Polyhedron 223 (2022) 115945

Contents lists available at ScienceDirect

Polyhedron

journal homepage: www.elsevier.com/locate/poly

Structural variety, fluorescence and photocatalytic activity of dissymmetric thiosemicarbazone complexes

Cristina González-García [a,1], Cristina García-Pascual [a,1], Rodrigo Burón [a], David G. Calatayud [b], Josefina Perles [c], M. Antonia Mendiola [a,*], Elena López-Torres [a,*]

[a] Universidad Autónoma de Madrid, Departamento de Química Inorgánica, Cantoblanco 28049, Madrid, Spain
[b] Instituto de Cerámica y Vidrio, CSIC, 28049 Cantoblanco, Spain
[c] Single Crystal X-ray Diffraction Service, Servicio Interdepartamental de Investigación, Universidad Autónoma de Madrid, 28049 Cantoblanco, Spain

ARTICLE INFO

Keywords:
Thiosemicarbazone
Hydrazone
Crystal structure
Fluorescence
Photocatalytic activity

ABSTRACT

A new dissymmetric bis(thiosemicarbazone) ligand, H_2L^2, containing a 4-(1-naphthyl)-3-thiosemicarbazone branch has been easily prepared and characterized. The reactivity of this ligand and the hybrid isopropylthiosemicarbazone/naphtoylhydrazone, H_2L^1, with zinc(II), copper(II) and nickel(II) nitrates in the presence of different amounts of lithium hydroxide has been explored. The results show that although both ligands present two different acidic protons, the degree of deprotonation of the ligand cannot be selectively controlled, since in almost all the reactions carried out without base the ligand is at least singly deprotonated. Nevertheless, an interesting structural diversity is found, also influenced by the metal structural preferences, leading to the formation of monomeric (**1**–**5**, **8** and **9**), dimeric (**6**) and polymeric (**7**) species. The different degree of deprotonation of the ligands, together with the presence or the absence of nitrate ions and solvent molecules, lead to the formation of different supramolecular architectures based on different hydrogen bond arrays. Fluorescence spectroscopy in the solid state for the ligands and the complexes was performed and the results show that whereas H_2L^1 is fluorescent, for H_2L^2 no fluorescence emission was detected. Complexation of H_2L^1 leads, in general, to a quench of the fluorescence emission, except for complex [ZnL^1(EtOH)] **2**, which is much more fluorescent than the free ligand. Conversely, complexation of H_2L^2 with zinc(II) causes fluorescence emission. Photocatalytic experiments with the nickel and copper complexes shows that the four complexes can effectively degrade methyl orange under UV–vis irradiation.

1. Introduction

Thiosemicarbazones (TSCs) are a well-known class of organic ligands belonging to the family of Schiff bases. They have been extensively studied since they are very versatile molecules that present excellent chelating properties, leading to the formation of stable complexes that display outcoming applications in very different fields. Regarding the biological ones, TSCs ligands and their complexes exhibit, among others, anticancer [1–4], antimicrobial [5–8], antiviral [9–12] and antiparasitic [13–15] activities, but they can be used as well in the treatment of Alzheimer's disease [16–17] and as molecular imaging agents in the diagnosis of several malignancies [18–22]. In addition, TSCs have proved to be selective sensors for the determination of a wide range of metal ions [23–26] and possess fascinating structural properties due to the presence of both hard and soft donor atoms and acidic hydrogens that, in many cases can be selectively deprotonated [27–29], and to the possibility of modifying the ligand backbone to introduce pendant groups that confer interesting features such as fluorescence [25,30–32]. Recently, the use of symmetric bis(TSCs) ligands as electro and photocatalysts in Hydrogen Evolution Reactions (HER) has been described [33–36].

Within the TSCs, the bis(thiosemicarbazones) exhibit improved properties and introduce the possibility of designing dissymmetric ligands that can fit better the metal preferences or the requirements needed for a specific application. Although the synthesis of this kind of ligands can be very challenging due to many possible side-reactions such as symmetrization, cyclization or desulfurization [37–40], we have widely stablished experimental procedures for the selective synthesis of

* Corresponding authors. Tel.: +34 914974844 (M.A. Mendiola), +34 914972376 (E. López-Torres).
E-mail addresses: antonia.mendiola@uam.es (M.A. Mendiola), elena.lopez@uam.es (E. López-Torres).
[1] Both authors contribute equally.

https://doi.org/10.1016/j.poly.2022.115945
Received 26 April 2022; Accepted 29 May 2022
Available online 3 June 2022

these ligands and their complexes [28,41–44].

With the increase of industrialization, environmental pollution has become one outstanding challenge for the sustainable development of human society. Organic dyes, such as rhodamine B (RhB), methyl orange (MO), methylene blue (MB) or congo red (CR) released from the textile, rubber and printing industries, are one of the main pollutants in industrial wastewater due to their toxicity and accumulation [45]. The spillage of such pollutants into rivers can destroy the environmental and ecological systems and have a negative effect in both aquatic organisms and the human health. Most dyes are very difficult to degrade by heat or conventional treatments because of the presence of π-conjugated systems. Therefore, the efficient removal of organic dyes from wastewater is an important topic to pursue. Adsorption, filtration, coagulation, chemical precipitation, membrane separation or biodegradation are largely limited due to high maintenance costs and the formation of secondary pollutants [46–49]. Photodegradation has been investigated as one of the most effective methods for wastewater decontamination because it can decompose organic dyes under ultraviolet or visible light with low cost and high efficiency [50–52].

In this paper we report the synthesis and structural characterization, including topological analysis, of Ni(II), Cu(II) and Zn(II) complexes with one dissymmetric bis(thiosemicarbazone) ligand and one hybrid hydrazone/thiosemicarbazone. In addition, fluorescence studies in the solid state were used to evaluate the possibility of using both ligands as fluorescent sensors for these metals, and the photocatalytic activity of the nickel and copper complexes to degrade methyl orange was also tested.

2. Experimental

2.1. Materials and instrumentation

Microanalyses were carried out using a LECO CHNS-932 Elemental Analyzer. IR spectra in the 4000–400 cm^{-1} range were recorded as KBr pellets on a Jasco FT/IR-410 spectrophotometer. The ESI mass spectra in positive mode were recorded on a Q-STAR PULSAR I instrument using a hybrid analyzer QTOF (Quadrupole time-of-flight). Molar conductivity was measured using a freshly prepared DMF solution (ca. 10^{-3} M) at 25 °C with a Crison EC-Meter BASIC 30+ instrument. Magnetic susceptibility was carried out at room temperature using the Gouy method with a Sherwood Scientific balance. ^{1}H and ^{13}C NMR spectra were recorded on a spectrometer Bruker AVIII HD-300 MHz using DMSO-d_6 or acetone-d_6 as solvent and TMS as reference. ^{13}C CP/MAS NMR spectra were recorded at 298 K in a Bruker AV400WB spectrometer equipped with a 4 mm MAS (magic-angle spinning) NMR probe and obtained using a cross-polarization pulse sequence using spinning rates of 10–14 KHz, pulse delays of 30 s, contact times of 8 ms and TPPM (two-pulse phase-modulated) high power proton decoupling. Chemical shifts are reported relative to TMS and the CH of adamantane (29.5 ppm) as a secondary reference. Fluorescence spectroscopy measurements were performed in the solid state on a Varian Cary Eclipse Fluorescence spectrophotometer.

2.2. Synthesis of the compounds

All the chemicals were purchased from standard commercial sources and used as received.

4-isopropyl-3-thiosemicarbazide, **^{i}PrTSC.** It was prepared following the procedure previously described [44]. δH(300 MHz, DMSO-d_6, Me_4Si) 1.11 (6H, d, CH_3, *J* 6.6), 4.35 (1H, m, CH), 4.40 (2H, s, NH_2), 7.45 (1H, d, N*H*-^{i}Pr, *J* 8.6), 8.48 (1H, s, NH).

Diacetyl-2-(4-isopropyl-3-thiosemicarbazone), **HA^{i}PrTSC** [44]. δH (300 MHz, DMSO-d_6, Me_4Si) 1.23 (6H, d, CH_3-^{i}Pr, *J* 6.6), 1.95 (3H, s, CH_3-CN), 2.40 (3H, s, CH_3-CO), 4.48 (1H, m, CH-^{i}Pr), 8.11 (1H, d, N*H*-^{i}Pr, *J* 8.4), 10.56 (1H, s, NH). Crystals suitable for single crystal X-ray analysis were obtained by slow evaporation of the mother liquor.

4-(1-naphthyl)-3-thiosemicarbazide, **NfTs.** To a solution of 2.51 g (13.6 mmol) of 1-naphthylisothiocyanate in 20 mL of diethyl ether was added 1.0 mL (20.6 mmol) of hydrazine monohydrate. The mixture was stirred for 30 min at room temperature. The white solid was filtered off, washed thoroughly with diethyl ether and vacuum-dried (2.88 g, 98%). δH(300 MHz, DMSO-d_6, Me_4Si) 9.23 (1H, s, H_{6A}), 7.99–7.51 (7H, m, H_6-H_{13}), 7.49 (1H, s, H_5), 3.35 (2H, s, NH_2).

Diacetyl-2-(4-isopropyl-3-thiosemicarbazone)-3-(3-hydroxy-2-naphthohydrazone), **H_2L^1** [44]. ν_{max}/cm^{-1} 3522 (OH), 3359, 3342 and 3178 (NH), 1645 (CO), 1628, 1523 and 1496 (CN + thioamide I + amide II) and 813 (thioamide IV). δH(300 MHz, DMSO-d_6, Me_4Si) 11.78 (1H, s, H_{2A}), 11.61 (1H, s, H_5), 10.21 (1H, s, H_2), 8.62 (1H, s, H_6), 7.97 (2H, m, H_1 + H_8), 7.76 (1H, d, H_{11}, *J* 8.2), 7.51 (1H, t, H_{10}, *J* 7.3), 7.37 (2H, m, H_9 + H_{13}), 4.50 (1H, m, H_{17}), 2.26, 2.25 (3H, s; 3H, s, H_{15} and H_{16}), 1.24 (6H, d, H_{18} + H_{19}, *J* 6.7). δC(75.5 MHz, DMSO-d_6, Me_4Si) 177.2 (C_1), 161.7 (C_4), 153.0 (C_{14}), 148.6, 148.3, (C_2, C_3), 136.3 (C_{12}), 133.1 (C_7), 129.5 (C_6), 128.9 (C_5), 127.7 (C_8), 126.2 (C_{10}), 124.4 (C_{11}), 121.1 (C_9), 111.2 (C_{13}), 46.3 (C_{17}), 22.2 (C_{18} + C_{19}), 12.1, 11.8 (C_{15} and C_{16}).

Diacetyl-2-(4-isopropyl-3-thiosemicarbazone)-3-(1-naphthyl-3-thiosemicarbazone), **H_2L^2.** A solution of 0.83 g (3.8 mmol) of 4-(1-naphthyl)-3-thiosemicarbazide in 10 mL of ethanol was added to a suspension of 0.77 g (3.80 mmol) of HA^{i}PrTSC in 20 mL of the same solvent with eight drops of conc. hydrochloric acid. The mixture was stirred for 4 h and the creamy precipitate was filtered off, washed with ethanol and vacuum-dried (1.36 g, 89%). Found: C, 56.8; H, 6.0; N, 21.1; S, 15.9. $C_{19}H_{24}N_6S_2$ requires C, 57.0; H, 6.0, N, 21.0; S, 16.0. ν_{max}/cm^{-1} 3320, 3271 and 3181 (NH), 1616 and 1597 (CN + thioamide I) and 806 (thioamide IV). 10.74 (1H, s, H_{6A}), 10.25 (1H, s, H_5), 10.20 (1H, s, H_2), 8.00–7.80 (5H, m, H_{13} + H_1 + H_{10} + H_8 + H_{12}), 7.56 (3H, m, H_{11} + H_7 + H_6), 4.52 (1H, m, H_{17}), 2.33 (1H, s, H_{16}), 2.29 (1H, s, H_{15}), 1.25 (6H, d, H_{18} + H_{19}, *J* 6.6). δC(75.5 MHz, DMSO-d_6, Me_4Si) 179.1 (C_4), 176.9 (C_1), 149.4, 148.6 (C_3 and C_2), 135.9 (C_5), 134.1 (C_9), 130.7 (C_{10}), 128.6 (C_7), 127.5 (C_{11}), 126.7 (C_{12}), 126.5 (C_{13} + C_{14}), 125.9 (C_8), 123.5 (C_6), 46.3 (C_{17}), 22.4 (C_{18} + C_{19}), 12.5, 12.2 (C_{15} and C_{16}).

All the complexes were synthesised by addition of the corresponding metal salt dissolved in 5 mL of ethanol onto a suspension of H_2L^1 or H_2L^2 in 20 mL of the same solvent in a 1:1 M ratio and in the absence or in the presence of one or two equivalents of LiOH·H_2O The mixture was stirred for several hours under reflux or at room temperature. The solid formed was filtered off, washed with ethanol and vacuum-dried.

$[Zn(HL^1)(OH_2)]NO_3$ (1). H_2L^1 (0.300 g, 0.78 mmol), $Zn(NO_3)_2{\cdot}6H_2O$ (0.230 g, 0.78 mmol), refluxed for 24 h, yellow-orange solid (0.278 g, 68%). Λ_M ($cm^2/\Omega mol$, DMF): 73.3. Found: C, 43.15; H, 4.7; N, 15.9; S, 6.2. $ZnC_{19}H_{24}N_6SO_6$ requires C, 43.0; H, 4.6, N, 15.9; S, 6.0. ν_{max}/cm^{-1} 3232 (OH + NH), 1647 (CO), 1550 (CN + thioamide I + amide II), 1385 (NO) and 819 (thioamide IV). δH(300 MHz, DMSO-d_6, Me_4Si) 11.76 (1H, s, H_{2A}), 11.61 (1H, s, H_5), 10.21 (1H, s, H_2), 8.62 (1H, s, H_6), 7.96 (2H, m, H_1 + H_8), 7.76 (1H, d, H_{11}, *J* 8.3), 7.51 (1H, t, H_{10}, *J* 7.3), 7.37 (2H, m, H_9 + H_{13}), 4.50 (1H, m, H_{17}), 2.26, 2.23 (3H, s; 3H, s, H_{15} and H_{16}), 1.23 (6H, d, H_{18} + H_{19}, *J* 6.7). δC(75.5 MHz, DMSO-d_6, Me_4Si) 177.1 (C_1), 160.8 (C_4), 152.9 (C_{14}), 148.7, 148.4, (C_2, C_3), 136.5 (C_{12}), 133.7 (C_7), 129.4 (C_6), 127.9 (C_5), 127.1 (C_8), 125.9 (C_{10}), 124.8 (C_{11}), 118.8 (C_9), 111.8 (C_{13}), 50.5 (C_{17}), 22.8, 22.4 (C_{18}, C_{19}), 16.2, 15.4 (C_{15} and C_{16}). ESI^+ *m/z*: 448.08 $[Zn(HL^1)]^+$. Crystals suitable for single crystal X-ray diffraction were obtained by slow evaporation of the mother liquor. This complex was also obtained with similar yield in the presence of one equivalent of LiOH·H_2O.

$[ZnL^1(EtOH)]$ (2). H_2L^1 (0.30 g, 0.78 mmol), LiOH·H_2O (0.070 g, 1.56 mmol), $Zn(NO_3)_2{\cdot}6H_2O$ (0.230 g, 0.78 mmol), 24 h under reflux, orange solid (0.233 g, 61%). Λ_M ($cm^2/\Omega mol$, DMF): 1.8. Found: C, 51.2; H, 5.7, N, 14.5; S, 6.5. $ZnC_{21}H_{27}N_5SO_3$ requires C, 50.95; H, 5.5; N, 14.2; S, 6.5. ν_{max}/cm^{-1} 3370 and 3271 (OH + NH), 1627 (CO), 1507 (CN + thioamide I + amide II) and 831 (thioamide IV). δH(300 MHz, DMSO-d_6, Me_4Si) 13.28 (1H, s, H_{2A}), 8.61 (1H, s, H_6), 7.90 (1H, d, H_8, *J* 8.1), 7.70 (1H, d, H_{11}, *J* 8.3), 7.59 (1H, s, H_1), 7.43 (1H, t, H_{10}, *J* 7.2), 7.27, 7.20 (1H, s; 1H, s, H_9 and H_{13}), 4.32 (1H, m, H_{17}), 2.31, 2.23 (1H, s; 1H, s, H_{15}

and H_{16}), 1.15 (6H, d, H_{18} + H_{19}, *J* 6.5). δC(75.5 MHz, DMSO-d_6, Me_4Si) 173.6 (C_1), 156.9 (C_4 + C_{14}), 150.8, (C_2 + C_3), 136.7 (C_{12}), 130.9 (C_7), 129.3 (C_6), 128.1 (C_5), 127.3 (C_8), 126.1 (C_{10}), 123.4 (C_{11}), 120.9 (C_9), 110.6 (C_{13}), 44.4 (C_{17}), 22.8 ($C_{18+}C_{19}$), 14.2, 13.8 (C_{15} and C_{16}). 56.5 (CH_3CH_2OH), 19.0 (CH_3CH_2OH). ESI^+ *m/z* 899.15 $[Zn_2(L^1)_2 + H]^+$, 448.08 $[ZnL^1 + H]^+$. Slow evaporation of the mother liquor yielded crystals suitable for single crystal X-ray diffraction. By recrystallization in DMSO, crystals of **[ZnL^1(DMSO)] 2a**, with DMSO instead of ethanol, were obtained.

[CuL^1] (**3**). H_2L^1 (0.30 g, 0.78 mmol), LiOH·H_2O (0.06 g, 1.56 mmol), $Cu(NO_3)_2$·$3H_2O$ (0.25 g, 0.79 mmol), 4 h at room temperature, dark brown solid. (0.360, 78%). Λ_M (cm^2/Ωmol, DMF): 17.1. Found: C, 50.9; H, 4.75, N, 15.5; S, 7.2. $CuC_{19}H_{21}N_5SO_2$ requires C, 51.0; H, 4.7, N, 15.7; S, 7.2. ν_{max}/cm^{-1} 3394, (OH + NH), 1639 (CO), 1571 (CN + thioamide I + amide II) and 819 (thioamide IV). ESI^+ *m/z* 447.08 $[M + H]^+$. Slow evaporation of the mother liquor yielded single crystals suitable for X-ray diffraction.

[NiL^1] (**4**). H_2L^1 (0.300 g, 0.78 mmol), $Ni(NO_3)_2$·$6H_2O$ (0.230 g, 0.79 mmol), 4 h at room temperature, reddish-brown solid (0.307 g, 88%). Λ_M (cm^2/Ωmol, DMF): 5.2. μ_{eff} (B. M.): 0. Found: C, 51.3; H, 4.6, N, 15.8; S, 7.1. $NiC_{19}H_{21}N_5SO_2$ requires C, 51.6; H, 4.8, N, 15.8; S, 7.2. ν_{max}/cm^{-1} 3332 (OH + NH), 1636 (CO), 1571 (CN + thioamide I + amide II), 826 (thioamide IV). δH(MHz, acetone-d_6, Me_4Si) 11.02 (1H, s, H_{2A}), 8.30 (1H, s, H_6), 7.90 (1H, d, H_8, *J* 8.2), 7.86 (1H, d, H_{11}, *J* 8.2), 7.71 (1H, s, H_1), 7.56 (1H, t, H_{10}, *J* 7.2), 7.47, 7.27 (1H, s; 1H, s, H_9 andH_{13}), 3.97 (1H, m, H_{17}), 2.53, 2.10 (1H, s; 1H, s, H_{15} and H_{16}). δC (75.5 MHz, DMSO-d_6, Me_4Si) 179.2, (C_1), 160.8 (C_4), 156.7 (C_{14}), 152.8, (C_2 + C_3), 137.6 (C_{12}), 135.2 (C_7), 129.3 (C_6), 127.0 (C_5), 124.5 (C_8), 119.7 (C_{10}), 110.5 (C_{11} + C_9), 108.4 (C_{13}), 50.2 (C_{17}), 21.1 (C_{18} + C_{19}), 16.6, 13.4 (C_{15} and C_{16}). ESI^+ *m/z* 443.04 $[M + H]^+$. Crystals suitable for single crystal X-ray analysis were formed by slow evaporation of a solution in acetone. The same complex was obtained, with similar yield, in the presence of LiOH·H_2O.

[Zn(H$_2$L^2)(ONO$_2$)] NO$_3$ (**5**). H_2L^2 (0.100 g, 0.26 mmol), Zn $(NO_3)_2$·$6H_2O$ (0.076 g, 0.26 mmol), 1 h at room temperature, yellow solution. A yellow solid was obtained by slow evaporation of the solvent, (0.120 g, 80%). Λ_M (cm^2/Ωmol, DMF): 119.7. Found: C, 37.5; H, 4.5, N, 18.1; S, 10.3. $ZnC_{19}H_{24}N_8S_2O_6$ requires C, 37.55; H, 4.3, N, 18.4; S, 10.5. ν_{max}/cm^{-1} 3442 and 3212 (NH), 1652 and 1596 (CN + thioamide I), 1385 (NO) and 839 (thioamide IV). δH(300 MHz, DMSO-d_6, Me_4Si) 10.74 (1H, s, H_{6A}), 10.25 (1H, s, H_5), 10.20 (1H, s, H_2), 7.98 (1H, s, H_1), 8.00–7.53 (7H, m, H_{13} + H_{10} + H_8 + H_{12} + H_{11} + H_7 + H_6), 4.52 (1H, m, H_{17}), 2.30, 2.28 (1H, s; 1H, s, H_{15} and H_{16}), 1.25 (6H, d, H_{18} + H_{19}, *J* 6.6). δC(100.6 MHz, CP/MAS, Me_4Si) 180.9 (C_1), 175.4 (C_4), 146.4, 143.4, (C_3 and C_2), 134.5, 131.8, 131.0, 129.6, 127.6, 126.4 (C_5-C_{14}), 50.30 (C_{17}), 21.34, 19.95 (C_{18} and C_{19}), 16.6, 14.4 (C_{15} and C_{16}). ESI^+ *m/z* 463.07 $[ZnL^2 + H]^+$. ESI^- *m/z* 524.05 $[M-H]^-$. Attempts of recrystallisation in DMF afforded zinc(II) sulfate hexahydrate.

If the reaction was carried out stirring for 20 h, a yellow solid different to complex **5** was formed. Found: C, 42.85; H, 4.6, N, 18.5; S, 12.13. $ZnC_{19}H_{24}N_7S_2O_3$: requires C, 43.0; H, 4.4, N, 18.6; S, 12.1. Its recrystallisation in DMSO afforded crystals corresponding to complex $[Zn(HL^2)(\mu\text{-}O_2SO_2)Zn(HL^2)]$ (**6**). This complex was also synthesized in good yield from $ZnSO_4$·$6H_2O$ (*vide infra*).

[Zn(HL^2)(μ-O$_2$SO$_2$)Zn(HL^2)] (**6**). H_2L^2 (0.100 g, 0.26 mmol), $ZnSO_4$·$6H_2O$ (0.076 g, 0.26 mmol), 1 h under reflux, yellow solid. (0.098, 75%). Λ_M (cm^2/Ωmol, DMF): 40.3. Found: C, 44.85; H, 4.5, N, 15.8; S, 15.5. $Zn_2C_{38}H_{48}N_{12}S_5O_4$ requires C, 44.95; H, 4.5, N, 15.9; S, 15.6. ν_{max}/cm^{-1} 3434, 3259 and 3207 (NH), 1637, 1577 and 1539 (CN + thioamide I), 1164, 1101 and 1037 (SO) and 845 (thioamide IV). δC (100.6 MHz, CP/MAS, Me_4Si) 179.6, 178.6 (C_4), 173.9 (C_1), 150.92, 148.00, 145.79 (C_2 and C_3), 134.2, 128.4, 127.7, 125.3, 124.4, 123.0, 122.8, 118.9, 118.1 (C_5-C_{14}), 48.92, 47.69 (C_{17}), 24.48, 22.18, 20.48 (C_{18} and C_{19}), 13.6, 13.0 (C_{15} and C_{16}).

[ZnL^2]$_n$ (**7**). H_2L^2 (0.100 g, 0.26 mmol), LiOH·H_2O (0.022 g, 0.52 mmol), $Zn(NO_3)_2$·$6H_2O$ (0.076 g, 0.26 mmol), 1 h at room temperature, pale orange solid. (0.088 g, 74%). Found: C, 49.0; H, 4.8, N, 18.3; S, 14.0. $ZnC_{19}H_{22}N_6S_2$ requires C, 49.2; H, 4.8; N, 18.1; S, 14.1. ν_{max}/cm^{-1} 3445, (NH), 1594, 1575 and 1556 (CN + thioamide I) and 841 (thioamide IV). δH(300 MHz, DMSO-d_6, Me_4Si) 9.23 (1H, s, H_{6A}), 8.01 (1H, m, H_{13}), 7.91 (1H, m, H_{10}), 7.69 (2H, m, H_8 + H_{12}), 7.49 (3H, m, H_6 + H_7 + H_{11}), 7.22 (1H, s, H_1), 4.50 (1H, m, H_{17}), 2.18, 2.05 (1Hs; 1H, s, H_{15} and H_{16}), 1.14 (6H, d, H_{18} + H_{19}, *J* 6.5). δC(75.5 MHz, DMSO-d_6, Me_4Si) 176.0 (C_1 + C_4), 148.2, (C_2 + C_3), 136.6 (C_5), 134.1 (C_9), 129.1 (C_{10}), 128.3 (C_7), 126.2 (C_{11}), 125.9 (C_{12}), 125.8 (C_{14}), 125.0 (C_{13}), 124.0 (C_8), 123.3 (C_6), 44.1 (C_{17}), 22.9 (C_{18} + C_{19}), 14.6, 14.2 (C_{15} and C_{16}). ESI^+ *m/z* 453.07 $[ZnL^2 + H)]^+$. Slow evaporation of the mother liquor yielded crystals suitable for single crystal X-ray diffraction.

[CuL^2] (**8**). H_2L^2 (0.100 g, 0.26 mmol), LiOH·H_2O (0.022 g, 0.52 mmol), $Cu(NO_3)_2$·$3H_2O$ (0.060 g, 0.26 mmol), 1 h at room temperature, reddish-brown solid. (0.081 g, 70%). Λ_M (cm^2/Ωmol, DMF) 2.1. Found: C, 49.4; H, 4.8; N, 17.9; S, 13.7. $CuC_{19}H_{22}N_6S_2$ requires C, 49.4; H, 4.8; N, 18.2; S, 13.8. ν_{max}/cm^{-1} 3446 and 3365 (NH), 1594 and 1579 (CN + thioamide I) and 840 (thioamide IV). ESI^+ *m/z* 462 $[M + H]^+$.

[NiL^2] (**9**). H_2L^2 (0.100 g, 0.26 mmol), $Ni(NO_3)_2$·$6H_2O$ (0.062 g, 0.26 mmol), 1 h at room temperature, dark green solid. (0.092 g, 81%). Λ_M (cm^2/Ωmol, DMF) 3.2. μ_{eff} (B. M.) 0. Found: C, 50.1; H, 5.2; N, 18.3; S, 13.7. $NiC_{19}H_{22}N_6S_2$ requires C, 49.9; H, 4.9; N, 18.4; S, 14.0. ν_{max}/cm^{-1} 3396 and 3287 (NH), 1577, 1560 and 1540 (CN + thioamide I) and 858 (thioamide IV). δH(300 MHz, DMSO-d_6, Me_4Si) 9.95 (1H, s, H_{6A}), 7.97 (2H, m, H_{10} + H_8), 7.78 (1H, d, H_{13}, *J* 7.2), 7.49 (4H, m, H_6 + H_7 + H_{11} + H_{12}), 7.48 (1H, s, H_1), 3.88 (1H, m, H_{17},), 1.92, 1.85 (1H, s; 1H, s, H_{15} and H_{16}), 1.08 (6H, d, H_{18} + H_{19}, *J* 5.9). δC(75.5 MHz, DMSO-d_6, Me_4Si) 177.46 (C_1 + C_4), 155.15, (C_2 + C_3), 136.4 (C_5), 133.7 (C_9), 129.0 (C_{10}), 128.4 (C_7), 126.6 (C_{11}), 126.5 (C_{12}), 126.3 (C_{14}), 125.8 (C_{13}), 124.2 (C_8), 123.6 (C_6), 48.15 (C_{17}), 22.48 (C_{18} + C_{19}), 14.45, 14.15 (C_{15} and C_{16}). ESI^+ *m/z* 457.08 $[M + H]^+$. Slow evaporation of a solution in DMSO yielded crystals suitable for single crystal X-ray diffraction. The same complex was obtained, with similar yield, in the presence of LiOH·H_2O.

2.3. Testing of photocatalytic activity

The photocatalytic activity of the prepared copper and nickel complexes was evaluated using the following methodology: 50 mg of the complex was suspended in 50 mL of an aqueous solution of methyl orange 10^{-5} M using a quartz beaker for UV–vis irradiation. The suspension, kept under magnetic stirring, was then irradiated using a high-pressure mercury vapor lamp for UV–vis irradiation (250 W, HPL-N Philips, Amsterdam, The Netherlands). 4 mL aliquots were taken progressively from the suspension after different irradiation time and their absorption spectrum was measured on the spectrometer, and the concentration (degradation) of methyl orange (MO) was determined by monitoring the changes in the absorbance at 465 nm. On collecting these data, two side effects were considered in order to avoid a misinterpreted decreased value in the MO concentration: the self-degradation of the MO molecule under the irradiation, and/or its degradation in the absence of light (non-photocatalytic degradation). Both scenarios were contemplated as follows: on the one hand, a blank solution of MO with no complex was irradiated under the same experimental conditions; as it was observed, in the absence of the complex, no degradation of MO was indeed produced. On the other hand, suspensions with MO and the different complexes were prepared as described before but they were not subjected to irradiation: in such dark conditions, no changes in the MO concentration were observed for these suspensions all throughout the test, so non-photocatalytic degradation was discarded in all cases. The experiments were repeated three times observing in all cases a statistical uncertainty below 1%.

2.4. Crystallographic data and structure determination

Crystallographic data were collected at room temperature on a

Bruker Kappa Apex II diffractometer equipped with an Apex-II CCD area detector using a graphite monochromator (Mo k_α radiation, $\lambda = 0.71073$ Å). The substantial redundancy in data allows empirical absorption corrections (SADABS) [53] to be applied using multiple measurements of symmetry-equivalent reflections. The raw intensity data frames were integrated with the SAINT program, which also applied corrections for Lorenz and polarization effects [54].

The software package SHELXTL version 6.10 was used for space group determination, structures solution and refinement. The structures were solved by direct methods (SHELXS-97) [55], completed with difference Fourier syntheses, and refined with full-matrix least squares using SHELXL-97 or 2014 minimizing $\omega(F_0^2 - F_c^2)$. Weighted R factors (R_w) and all goodness of fit S area based on F^2; conventional R factors (R) are based on F [56]. All non-hydrogen atoms were refined with anisotropic displacements parameters. The hydrogen atoms bonded to carbon atoms were positioned geometrically and those on nitrogen and oxygen atoms were located in a difference Fourier map and their coordinates and isotropic thermal parameters subsequently refined. All scattering factors and anomalous dispersions factors are contained in the SHEXTL 6.10 program library. For complex **1** the hydrogen atoms of the molecules of water could not be located in the difference Fourier map, presumably as a result of disorder. They have been omitted from the model but included in calculations of the formula, weight etc.

3. Results and discussion

3.1. Synthesis

A new dissymmetric bis(thiosemicarbazone) ligand H_2L^2 was synthesized by condensation of the mono thiosemicarbazone HA^iPrTSC with 4-(1-naphthyl)-3-thiosemicarbazide in ethanol at room temperature and in the presence of some drops of hydrochloric acid to catalyze the reaction.

Reactions of the hybrid thiosemicarbazone/hydrazone ligand H_2L^1 and the dissymmetric bis(thiosemicarbazone) H_2L^2 with zinc(II), copper (II) and nickel(II) nitrates were carried out in ethanol with none, one or two equivalents of lithium hydroxide. Pure complexes **1**–**9** (Schemes 1 and 2) were obtained in good yield under the reaction conditions described in the experimental part. In the reactions with zinc(II), complexes with the ligand acting as a neutral, singly and doubly deprotonated donor can be isolated, whereas with nickel(II) and copper(II) only complexes with the ligand fully deprotonated are obtained, even if no base is added to the reaction medium, due to the great stability of the square-planar complexes.

Reaction of H_2L^2 with $Zn(NO_3)_2{\cdot}6H_2O$ at room temperature for 20 h yields a yellow solid different to that isolated stirring for 1 h. Its analytical data agree with a 1:1:1, Zn:ligand:NO_3 molar ratio, which indicates the singly deprotonation of the ligand. By concentration of a solution of this solid in DMSO-d_6 for one week, a crystalline solid (**6**) was formed, which contains sulfate groups instead of the starting nitrate one. The same complex was synthesized directly by reaction of H_2L^2 with Zn $(SO_4)_2{\cdot}6H_2O$.

The mass spectra of the complexes show the peak corresponding to a metal plus one ligand, confirming the 1:1 stoichiometry. The values of the molar conductivity in DMF solution confirm that in complexes **1** and **5** one NO_3^- acts as a counter-ion. The relatively high value found for complex **5** compared to complex **1** (both 1:1 species) can be attributed to the partial solvolysis of the coordinated NO_3^- group by DMF, a solvent with a high coordinating ability, increasing the conductivity observed in DMF solution. Conversely, complexes **2**, **3**, **4**, **6**–**9** are molecular species, although the value observed for complex 6 is considerably higher than for the other compounds. This can be explained by the presence of a SO_4^{2-} anion in complex **6** that can be replaced by DMF increasing the conductivity. By contrast, the other molecular species do not contain any anion that can be replaced by the solvent, so the resulting conductivity is considerably lower [57]. Magnetic susceptibilities for the nickel(II) complexes at room temperature support their square-planar geometry.

3.2. Crystal structures

The molecular structure of H_2A^iPrTs and eight complexes has been determined by single crystal X-ray diffraction. Significant crystal structure and refinement data are listed in Tables 1 and 2 and relevant bond distances and angles in the in the metal coordination environments are summarized in Tables 3 and 4.

The molecular structure of the monoketone H_2A^iPrTs (S.1) exhibits a *E* disposition around de C—C bond and the azometine nitrogen and the sulfur atom are also in *E*. The molecules are forming dimers through hydrogen bonds between the hydrazinic nitrogen and the sulfur atoms.

In all the complexes the ligands behave as N_2SO or N_2S_2 tetradentate chelates, coordination mode that leads to the formation of three five-member chelate rings that confers high stability to the complexes.

The asymmetric unit of the crystal structure of complex **1** contains two crystallographically-distinct molecules of $[Zn(HL^1)(OH_2)]^+$, two nitrates and one ethanol and one water molecules of crystallization. The two cations are geometrically very similar in which the ligand is monodeprotonated by the loss of the hydrazinic hydrogen of the hydrazone branch. The zinc(II) ions are penta-coordinated with one tetradentate ligand and one molecule of water in a square-based pyramid arrangement (Fig. 1) with $\tau_5 = 0.00$ for Zn1 and $\tau_5 = 0.01$ for Zn2 ($\tau_5 = 0$ for sbp and $\tau_5 = 1$ for tbp) [58]. Both ligands skeleton, including the naphthol rings, can be considered planar with the Zn(II) ions located 0.409 and 0.404 Å, for Zn1 and Zn2 respectively, above the least-squares plane. The main difference amongst the cations consists of the orientation of the OH groups, whilst in the ligand coordinated to Zn1 is pointing to the deprotonated hydrazinic nitrogen, leading to the formation of an

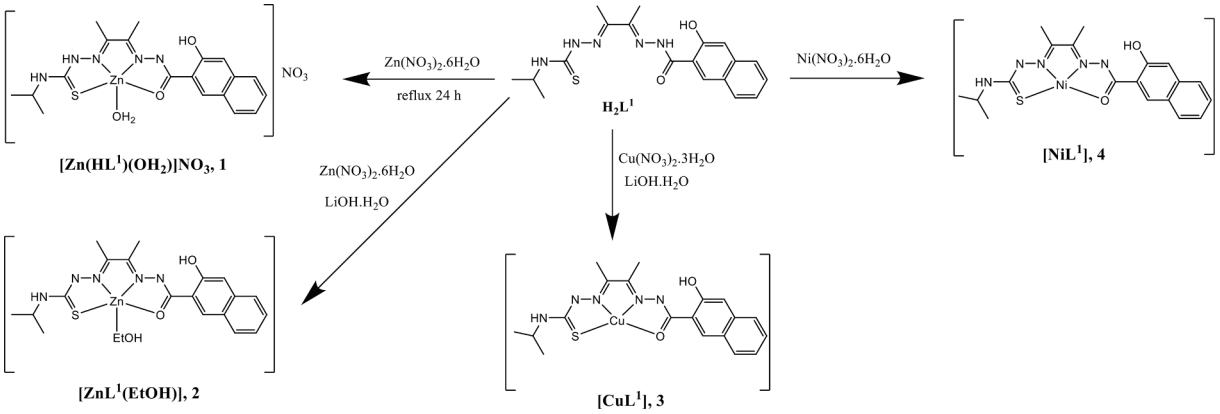

Scheme 1. Synthesis of the complexes derived from H_2L^1.

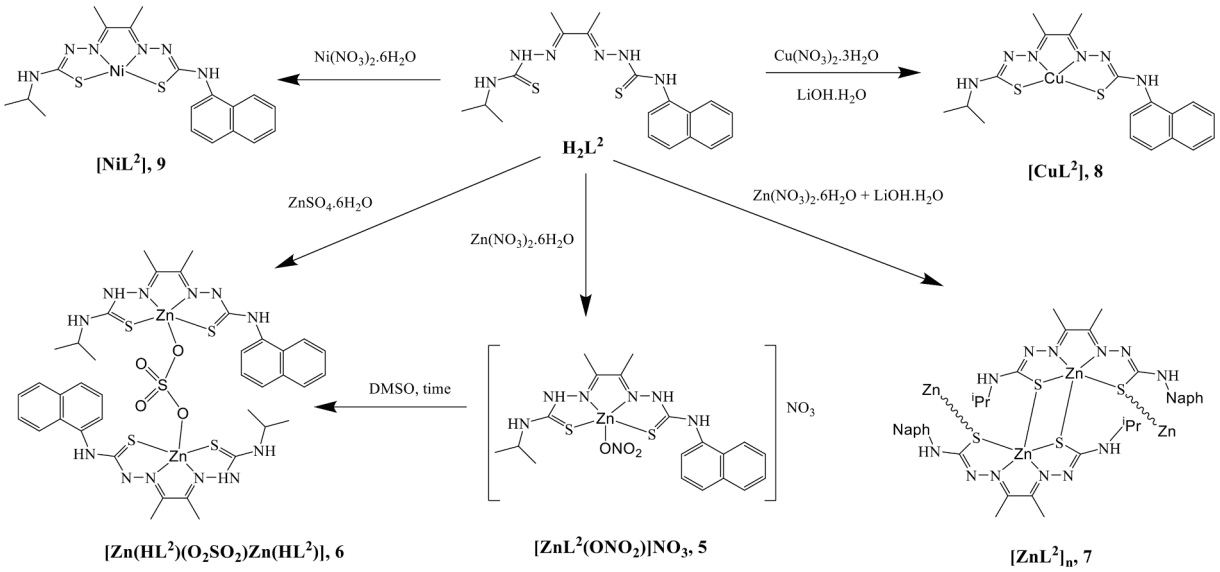

Scheme 2. Synthesis of the complexes derived from H_2L^2.

Table 1
Crystallographic data and refinement of HA^{i}PrTSC and complexes **1**.EtOH·H_2O, **2**, **2a** and **3**.

	HA^{i}PrTSC	1.EtOH·H_2O	2	2a	3
Formula	$C_8H_{15}N_3OS$	$ZnC_{20}H_{28}N_6O_7SZn$	$ZnC_{21}H_{27}N_5O_3S$	$ZnC_{21}H_{27}N_5O_3S_2$	$CuC_{19}H_{21}N_5O_2S$
M	201.29	561.91	494.90	526.96	447.01
Temperature/K	296(2)	296(2)	296(2)	296(2)	2963(2)
Crystal system	Triclinic	Monoclinic	Monoclinic	Triclinic	Triclinic
Space group	$\bar{P}1$	P 21/c	P 21/c	$\bar{P}1$	$\bar{P}1$
a/Å	6.055(4)	16.325(3)	11.4640(2)	11.3032(3)	8.7207(7)
b/Å	9.863(9)	23.596(4)	11.6034(2)	11.8618(3)	8.8805(6)
c/Å	10.883(6)	13.908(3)	18.4232(4)	18.0935(4)	14.4673(12)
α/°	113.37(4)	90	90	90.2410(10)	73.343(3)
β/°	106.12(3)	108.968(6)	107.6840(10)	97.1620(10)	73.448(4)
γ/°	94.53(5)	90	90	91.2380(10)	65.492(3)
U/ Å^3	559.8(7)	5066.3(16)	879.02(7)	2406.36(9)	958.82(13)
Z	2	8	4	4	2
D_c/Mgm^{-3}	1.194	1.473	1.408	1.455	1.548
Absorption coefficient mm^{-1}	0.259	1.103	1.173	1.226	1.274
F(000)	604	2336	1032	1096	462
Goodness of fit on F^2	1.035	1.051	0.999	1.000	1.041
Reflections collected	9234	52,550	45,738	76,016	28,337
Independent reflections	2032 [R(int) = 0.0251]	9376[R(int) = 0.1389]	4786[R(int) = 0.0514]	11,807 [R(int) = 0.0341]	3500 [R(int) = 0.0512]
Final R1and w$R2$[I > 2σ(I)]	0.0384, 0.1225	0.0750, 0.1788	0.0335, 0.0845	0.0352, 0.0970	0.0418, 0.1167
R indices (all data)	R1 = 0.0519, w$R2$ = 0.1329	R1 = 0.1765, w$R2$ = 0.2314	R1 = 0.0613, w$R2$ = 0.0975	R1 = 0.0573, w$R2$ = 0.1084	R1 = 0.0644, w$R2$ = 0.1275
Residual electron density (min,max) (eÅ^{-3})	−0.165, 0.239	−0.914, 0.647	−0.259, 0.323	−0.318, 0.903	−0.294, 0.392

intramolecular hydrogen bond, in the ligand bound to Zn2 is rotated and forming a hydrogen bond with the crystallization water molecule. There is an extended network of hydrogen bonds involving the amine groups, the water molecules, the nitrate ions and the ethanol molecule, which is discussed in the topological analysis section.

The crystal structure of complex **2** (Fig. 2) is made up of discrete molecules of [ZnL^1(EtOH)] with the Zn(II) ion coordinated to one doubly deprotonated ligand and an ethanol molecule in a square-based pyramid environment ($\tau_5 = 0.01$), with the metal ion 0.381 Å above the ligand skeleton least-squares plane. There is an intramolecular hydrogen bond between the OH group of the ligand and the deprotronated hydrazinic nitrogen N5, as well as intermolecular hydrogen bonds connecting the ethanol molecules with the OH and the NH with the C═O groups leading to a 3D network (*vide infra*). When complex **2** is recrystallized in DMSO substitution of the ethanol by an O-coordinated DMSO molecule takes place leading to the isolation of complex **2a** (Fig. 2). The asymmetric unit of this complex contains two crystallographically independent molecules of [ZnL^1(DMSO)] that do not present significant differences and in which the Zn(II) ions are in a coordination environment analogous to that of complex **2** ($\tau_5 = 0.00$ for Zn1 and $\tau_5 = 0.05$ for Zn2). The main difference among these two complexes is the intermolecular H bond network, since DMSO is not involved in it and the molecules form a 2D architecture.

The crystal structures of complexes **3** and **4** (Fig. 3) show discrete molecules of [ML^1] with the metal ions coordinated to a dianionic ligand in a square-planar arrangement with $\tau_4 = 0.24$ for Cu1 and $\tau_4 = 0.16$ for Ni1 ($\tau_4 = 0$ for sp and $\tau_4 = 1$ for Td) [59]. This deviation from the ideal value of 0 arises from the asymmetry in the bite angles of the ligand, since the S-M−O is much wider that the other three, but the ligand skeleton and the metal ions are coplanar. The main difference between the two structures is the presence of intermolecular H bonds in complex **4** that lead to the formation of chains running parallel to the *b* axis.

The molecular structure of complex **6** (Fig. 4) reveals it is a dinuclear complex in which a bidentate sulfate anion is linking two [Zn(HL^2)]$^+$

Table 2
Crystallographic data and refinement of complexes **4**, **6**, **7** and **9**.DMSO.

	4	6	7	9.DMSO
Formula	$NiC_{19}H_{21}N_5O_2S$	$Zn_2C_{38}H_{46}N_{12}O_4S_5$	$ZnC_{19}H_{22}N_6S_2$	$NiC_{21}H_{28}N_6OS_3$
M	442.18	1025.91	463.91	535.38
Temperature/K	296(2)	296(2)	296(2)	296(2)
Crystal system	Monoclinic	Monoclinic	Triclinic	Monoclinic
Space group	P 21/c	P 21/n	*P*-1	P 21/c
a/Å	17.0801(11)	14.0214(4)	7.4629(3)	8.119(2)
b/Å	16.0419(9)	12.4292(4)	10.0472(3)	23.290(5)
c/Å	7.0942(5)	25.2967(7)	14.8025(5)	13.323(4)
α/°	90	90	93.845(2)	90
β/°	93.498(2)	92.434(2)	101.588(2)	102.3770(12)
γ/°	90	90	107.175(2)	90
U/ $Å^3$	1940.2(2)	4404.6(2)	1029.29(6)	2406.36(9)
Z	4	4	2	4
D_c/Mgm^{-3}	1.514	1.547	1.497	1.445
Absorption coefficient mm^{-1}	1.133	1.381	1.413	1.069
F(000)	920	2120	480	1120
Goodness of fit on F^2	1.096	0.981	1.077	1.510
Reflections collected	31,503	54,305	20,523	31,950
Independent reflections	3710 [R(int) = 0.0984]	8031[R(int) = 0.0840]	3749 [R(int) = 0.0401]	4498 [R(int) = 0.0342]
Final R1and w*R*2[I > 2σ(I)]	0.0495, 0.1121	0.0473, 0.1065	0.0551, 0.1461	0.0521, 0.1796
R indices (all data)	R1 = 0.1013, w*R*2 = 0.1481	R1 = 0.1008, w*R*2 = 0.1302	R1 = 0.0739, w*R*2 = 0.1594	R1 = 0.0620, w*R*2 = 0.1879
Residual electron density (min,max) ($eÅ^{-3}$)	−0.614, 0.524	−0.545, 0.766	−1.371, 2.018	−0.734, 2.439

Table 3
Selected bond distances and angles in complexes of H_2L^1.

	1. EtOH·H_2O	2	2a	3	4
M(1)-N(3)	2.175(6)	2.1343 (19)	2.1421 (17)	1.954(3)	1.840(3)
M(1)-N(4)	2.069(6)	2.0763 (18)	2.0618 (16)	1.929(3)	1.821(4)
M(1)-S(1)	2.345(2)	2.3075(6)	2.3407(6)	2.2246 (11)	2.1698 (13)
M(1)-O(1)	2.014(5)	2.1001 (15)	2.1058 (14)	1.984(3)	1.882(3)
M(1)-O(3)	2.009(5)	2.0763 (18)	2.0292 (15)	–	–
N(3)-M(1)-N(4)	71.8(2)	73.49(7)	73.61(7)	79.59(13)	83.51(16)
N(3)-M(1)-S(1)	81.17(17)	81.68(5)	80.24(5)	86.19(10)	87.36(12)
N(3)-M(1)-O(1)	146.0(2)	147.12(6)	147.00(6)	159.52 (12)	166.45 (15)
N(4)-M(1)-S(1)	146.00(17)	147.86(6)	147.19(5)	165.72(9)	170.87 (12)
N(4)-M(1)-O(1)	76.6(2)	75.33(7)	75.34(6)	79.97(11)	83.02(15)
O(1)-M(1)-S(1)	121.84(16)	122.32(5)	123.40(4)	114.21(8)	106.12 (10)
N(3)-M(1)-O(3)	106.5(2)	100.79(8)	108.64(7)	–	–
N(4)-M(1)-O(3)	105.8(2)	100.48(8)	106.16(7)	–	–
S(1)-M(1)-O(3)	101.33(16)	104.01(6)	100.68(4)	–	–
O(1)-M(1)-O(3)	93.8(2)	94.85(7)	90.48(6)	–	–

Table 4
Selected bond distances and angles in complexes of H_2L^2.

	6	7	9.DMSO
M(1)-N(3)	2.143(3)	2.107(3)	1.850(3)
M(1)-N(4)	2.118(3)	2.090(3)	1.856(3)
M(1)-S(1)	2.3992(12)	2.3619(12)	2.1556(11)
M(1)-S(2)	2.3405(12)	2.3763(12)	2.1460(11)
M(1)-O(2)	2.049(3)	–	–
M(1)-S(1)#1	–	2.9016(15)	–
M(1)-S(2)#2	–	2.9722(15)	–
N(3)-M(1)-N(4)	72.56(12)	74.65(13)	83.42(13)
N(3)-M(1)-S(1)	80.10(9)	81.00(10)	87.44(10)
N(3)-M(1)-S(2)	145.17(10)	153.46(10)	169.43(10)
N(4)-M(1)-S(1)	146.42(10)	154.68(10)	170.77(9)
N(4)-M(1)-S(2)	81.65(9)	80.79(10)	87.03(9)
S(1)-M(1)-S(2)	112.91(5)	124.36(4)	102.18(4)
N(3)-M(1)-O(2)/S(1)#1	102.87(13)	92.48(11)	–
N(4)-M(1)-O(2)/S(1)#1	94.80(13)	85.73(11)	–
S(1)-M(1)-O(2)/S(1)#1	110.24(9)	88.52(4)	–
S(2)-M(1)-O(2)/S(1)#1	102.23(8)	95.65(4)	–
N(3)-M(1)-O(2)/S(2)#2	–	83.41(11)	–
N(4)-M(1)-O(2)/S(2)#2	–	89.45(11)	–
S(1)-M(1)-O(2)/S(2)#2	–	94.62(4)	–
S(2)-M(1)-O(2)/S(2)#2	–	86.46(4)	–

Symmetry transformations used to generate equivalent atoms: #1 -x,-y + 2,-z + 2 #2 -x + 1,-y + 2,-z + 2.

units, leading to penta-coordinated Zn(II) ions with a distorted square-based pyramid geometry (τ_5 = 0.02 for Zn1 and 0.10 for Zn2), with the metal ions 0.553 Å (Zn1) and 0.561 Å (Zn2) above the ligand skeleton least-squares plane. The thiosemicarbazone ligand is singly deprotonated with the remaining hydrazinic nitrogen in the isopropyl arm. This can be confirmed by the CS and CN bond distances involving C1, C4, C20 and C23: in the deprotonated arm the values correlate well with an imine-thiol structure (C—S bond distances = 1.751 and 1.748 Å and C═N bond distances 1.306 and 1.309 Å), whereas in the non-deprotonated arm there is much more electronic delocalization, leading to CS bonds distances of 1.710 and 1.706 Å and CN bond distances of 1.368 and 1.59 Å. The naphthyl rings in the two $[Zn(HL^2)]^+$ units are located at opposite sides and they are canted 14.10 (C5-C14) and 13.42° (C24-C33) with respect to their corresponding thiosemicarbazone backbone, what was not observed in the crystal structures of complexes containing H_2L^1, in which the naphthol rings are coplanar with the rest of the ligand backbone due to the formation of an intramolecular hydrogen bond between the OH and the deprotonated nitrogen atom. The different degree of deprotonation of the thiosemicarbazone arms makes that the hydrogen atoms attached to *N*-isopropyl and *N*-naphthyl groups are pointing to different sides: in the arm with isopropyl it is on the same side than the hydrazinic hydrogen, whereas in the naphthyl one it is pointing to the sulfur atom. There are hydrogen bonds involving the hydrazinic protons, the NH^iPr and three of the oxygen atoms of the sulfate group, running along the *a* axis.

The crystal structure of complex **7** (Figs. 5 and 6) shows it is a polymeric complex in which the $[ZnL^2]$ units are connected through

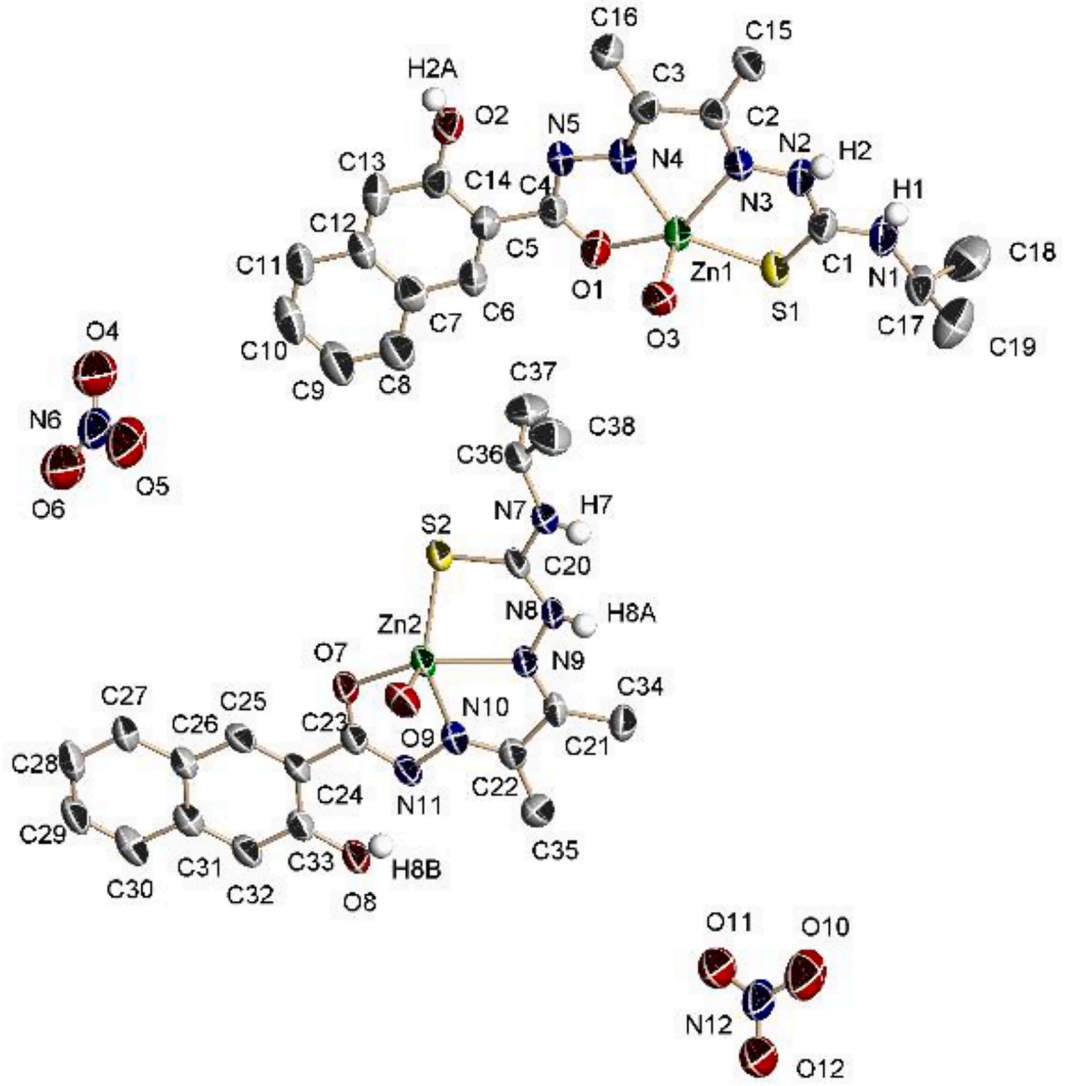

Fig. 1. Molecular structure of complex **[Zn(HL^1)(OH$_2$)]NO$_3$ 1**. Solvent molecules and some hydrogen atoms are omitted for clarity. Thermal ellipsoids at 50% probability level.

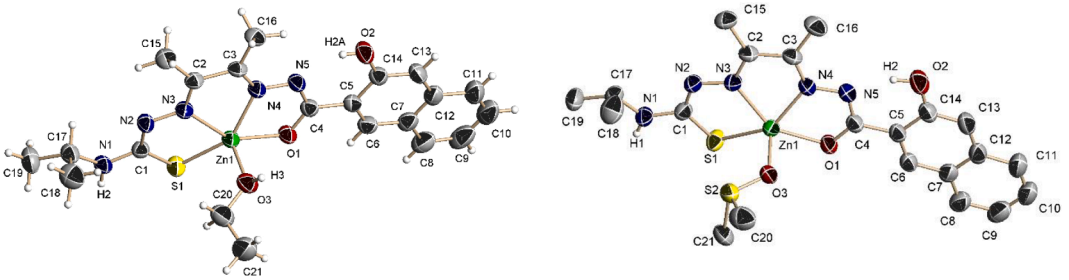

Fig. 2. Molecular structure of complexes **[ZnL^1(EtOH)] 2** (left) and **[ZnL^1(DMSO)] 2a** (right). Thermal ellipsoids at 50% probability level.

both sulfur atoms, each of them bonding to a different Zn(II) ion. In the polymer, the Zn(II) is *hexa*-coordinated in a N_2S_4 distorted octahedral environment. The ligand coordination mode induces that, to difference with the other complexes, the ligand is very deviated from planarity, with S1 0.317 Å under the ligand skeleton least-squares plane and Zn2 0.320 Å above the same plane. By contrast, both sulfur atoms pushing to opposite sides forces the zinc ion to be in the plane (deviation = 0.037 Å), what is not observed in the other zinc crystal structures described in this paper. The doubly deprotonation of the ligand makes that bond distances involving C1 and C4 corresponds to C═N (1.304 and 1.309 Å) and C—S (1.758 and 1.762 Å) and the naphthyl ring is rotated 12.44° with respect to the rest of the thiosemicarbazone. Double deprotonation in this complex makes that both NH groups are pointing to the sulfur atoms, what was observed in the deprotonated arm of complex **6**. In this complex there is not any supramolecular interaction.

Complex **9** crystallizes with one molecule of DMSO in the asymmetric unit, which is linked by hydrogen bonds with the NH groups. In the complex, the nickel(II) is coordinated to one doubly deprotonated

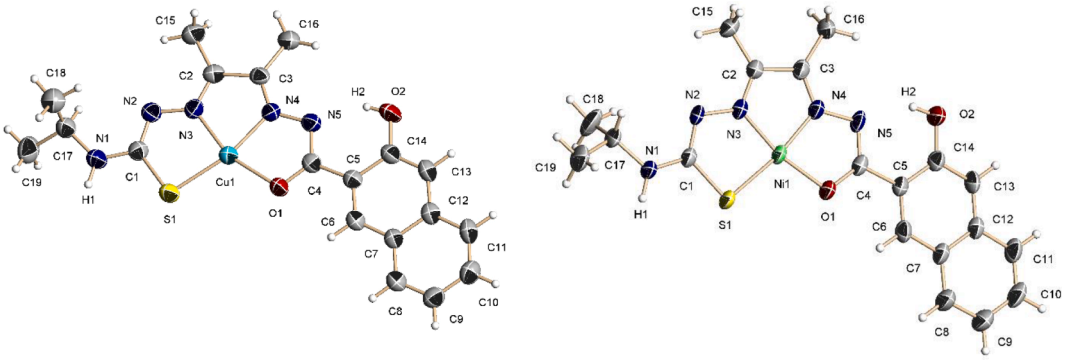

Fig. 3. Molecular structure of complexes **[CuL^1] 3** (left) and **[NiL^1] 4** (right). Thermal ellipsoids at 50% probability level.

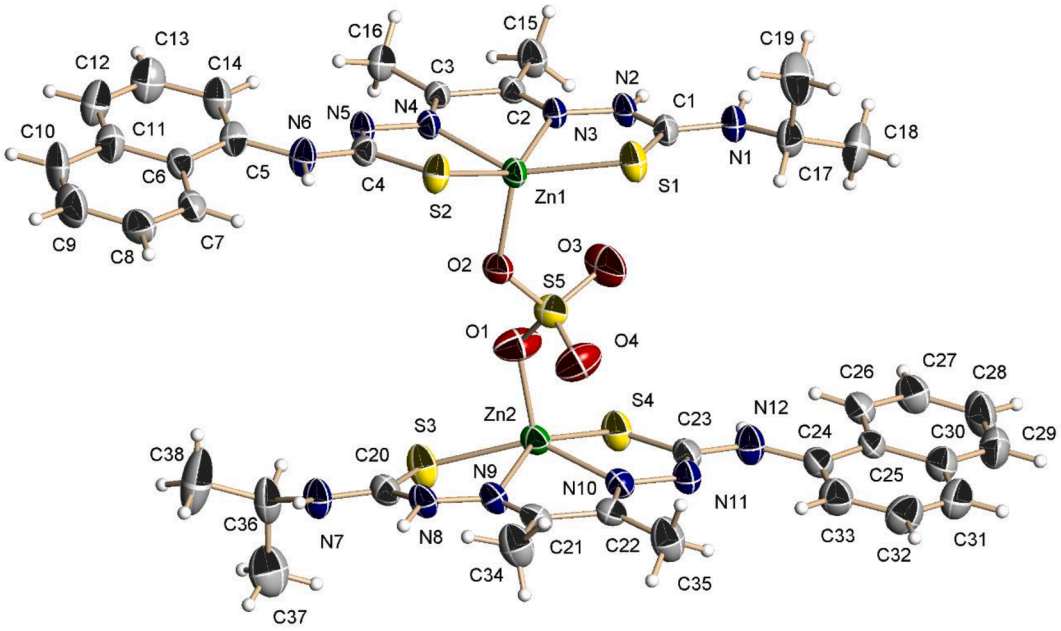

Fig. 4. Molecular structure of complex **[Zn(HL^2)(μ-O$_2$SO$_2$)Zn(HL^2)] 6**. Thermal ellipsoids at 50% probability level.

ligand in a square planar geometry (Fig. 7), with $\tau_4 = 0.14$, caused, as in complexes **3** and **5**, by the different bite angles of the ligand. The ligand, excluding the naphthyl ring, can be considered planar and the nickel is located in the plane. The naphthyl ring is twisted 15.98° with respect to the ligand core. As in complex **7**, both NH are located on the side of the sulfur atom.

3.3. Topological analysis

A comparative analysis of the supramolecular interactions in the crystal structures of compounds **1, 2, 2a, 3, 4, 6** and **9** was carried out with TOPOS [60]. For this comparison, the molecular species were considered as nodes, and the most relevant interactions between them as linkers (Tables S12-S18, in blue). The graphical representations of the underlying nets are collected in Fig. 8.

Compound **1** contains $[Zn(HL^1)(OH_2)]^+$ cations as well NO_3^- anions and solvent molecules (EtOH and H_2O). In this crystal structure, both hydrogen bonds and π-π interactions were found to be relevant, yielding zig-zag chains of cationic complexes in the [0 0 1] direction where the two crystallographically independent complexes containing Zn1 and Zn2 alternate. The resulting underlying net is a monodimensional uninodal biconnected net. Hydrogen bonds involving the cationic complexes and the anions and solvent molecules are also present, but these interactions do not contribute to the extension of the dimensionality of the supramolecular arrangement.

In the crystal of **2**, each [ZnL^1(EtOH)] molecule was found to be connected to four neighbour ones, considering both hydrogen bonds and π-π interactions, to yield a three-dimensional uninodal net with symbol 6^6 (**dia**). The analogous complex containing DMSO instead of EtOH, **2a**, presents a very different arrangement with [ZnL^1(DMSO)] molecules in layers parallel to the (1 0 1) plane joined by hydrogen bonds and π-π interactions. The underlying net is a uninodal two-dimensional tri-connected one with symbol 6^3 (**hcb**).

For compound **3,** no intermolecular H-bonds were found, and π-π interactions between each molecule and the two nearest neighbour ones give rise to zig-zag chains of [Cu(L^1)] complexes in the [1 0 0] direction resulting in a monodimensional uninodal biconnected net. In the case of the nickel derivative **4,** [NiL^1] molecules are joined by hydrogen bonds in the [0 1 0] direction and by π-π interactions in the [0 0 1] direction, yielding a uninodal tetraconnected two-dimensional underlying net of the **sql** type, with symbol $4^4 6^2$.

Compound **6** displayed both hydrogen bonds and weak π-π interactions between the dimetallic [Zn(HL^2)(μ-O$_2$SO$_2$)Zn(HL^2)] molecules, giving rise to straight chains in the [1 0 0] direction for a monodimensional uninodal biconnected net.

In the crystal structure of compound **9,** both [NiL^2] and interstitial DMSO molecules participate in the N—H···O hydrogen bonds to form zig-zag chains of alternating species in the [2 0 1] direction, giving rise to

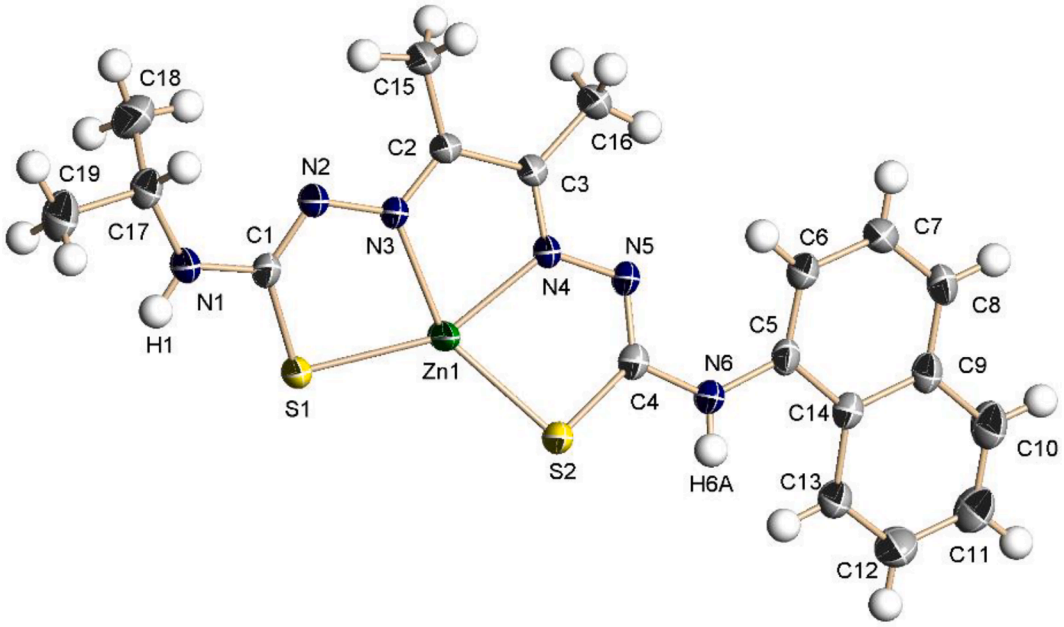

Fig. 5. Asymmetric unit of complex $[ZnL^2]_n$ **7**. Thermal ellipsoids at 50% probability level.

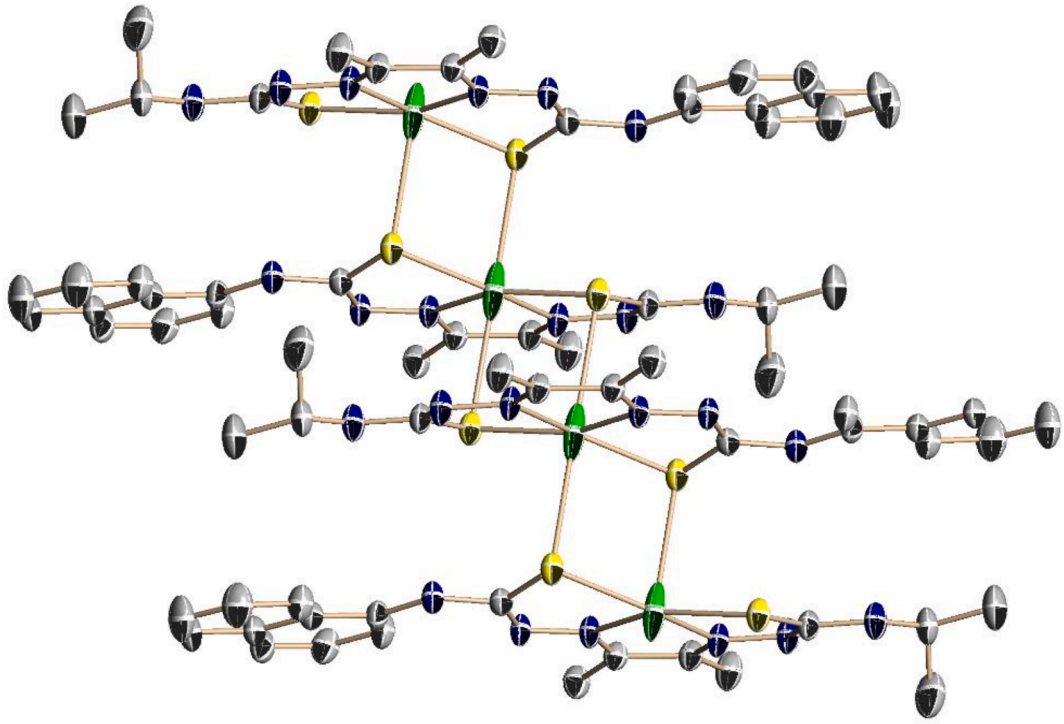

Fig. 6. View of the polymeric chain of complex $[ZnL^2]_n$ **7**. Thermal ellipsoids at 50% probability level.

a monodimensional uninodal biconnected underlying net.

Finally, the topological analysis was also applied to the polymeric structure of compound **7**, considering in this case the metal atoms as nodes and the ligands as linkers. The resulting underlying net was a monodimensional uninodal.

3.4. Spectroscopy

The IR spectrum of the ligand H_2L^2 shows the bands corresponding to the functional groups present in the molecule. The IR spectra of all the complexes, except complex **5** that contains a neutral ligand, provide evidence of the partial or total deprotonation of the NH groups. The shifts observed in the bands assigned to ν(CN), ν(CS) and ν(CO) are consistent with these groups being bonded to the metal ions, confirming that the ligands behave, at least, as N_2OS or N_2S_2 donors. Moreover, spectra of complexes **1** and **2** show additional bands corresponding to water or ethanol molecules and the bands corresponding to NO_3^- groups can be clearly observed in the spectra of complexes **1** and **5**. Finally, the IR spectra of complex **6** (both crystalline and powder solids) show several bands between 1200 and 1010 cm^{-1}, corresponding to the

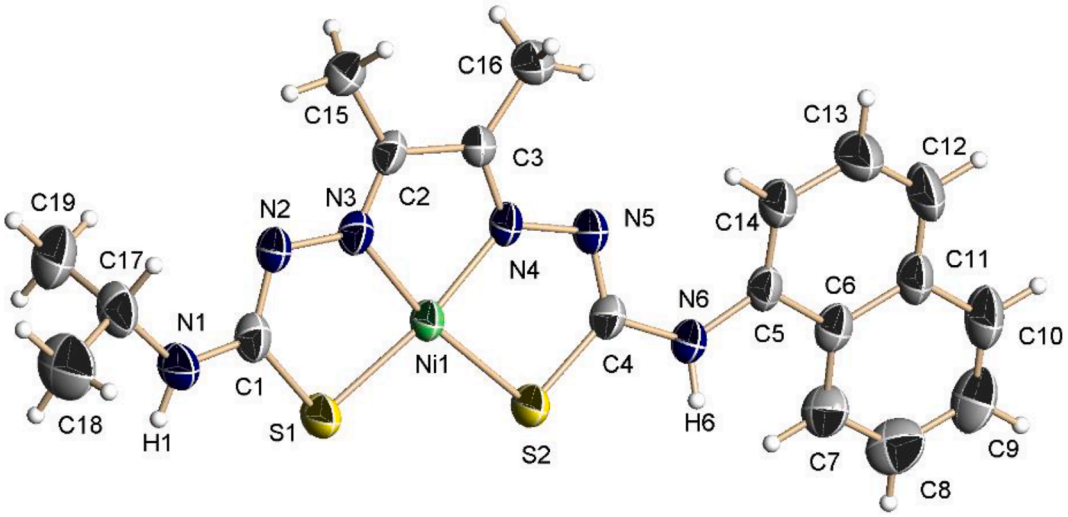

Fig. 7. Molecular structure of complex **[NiL^2] 9**. Thermal ellipsoids at 50% probability level.

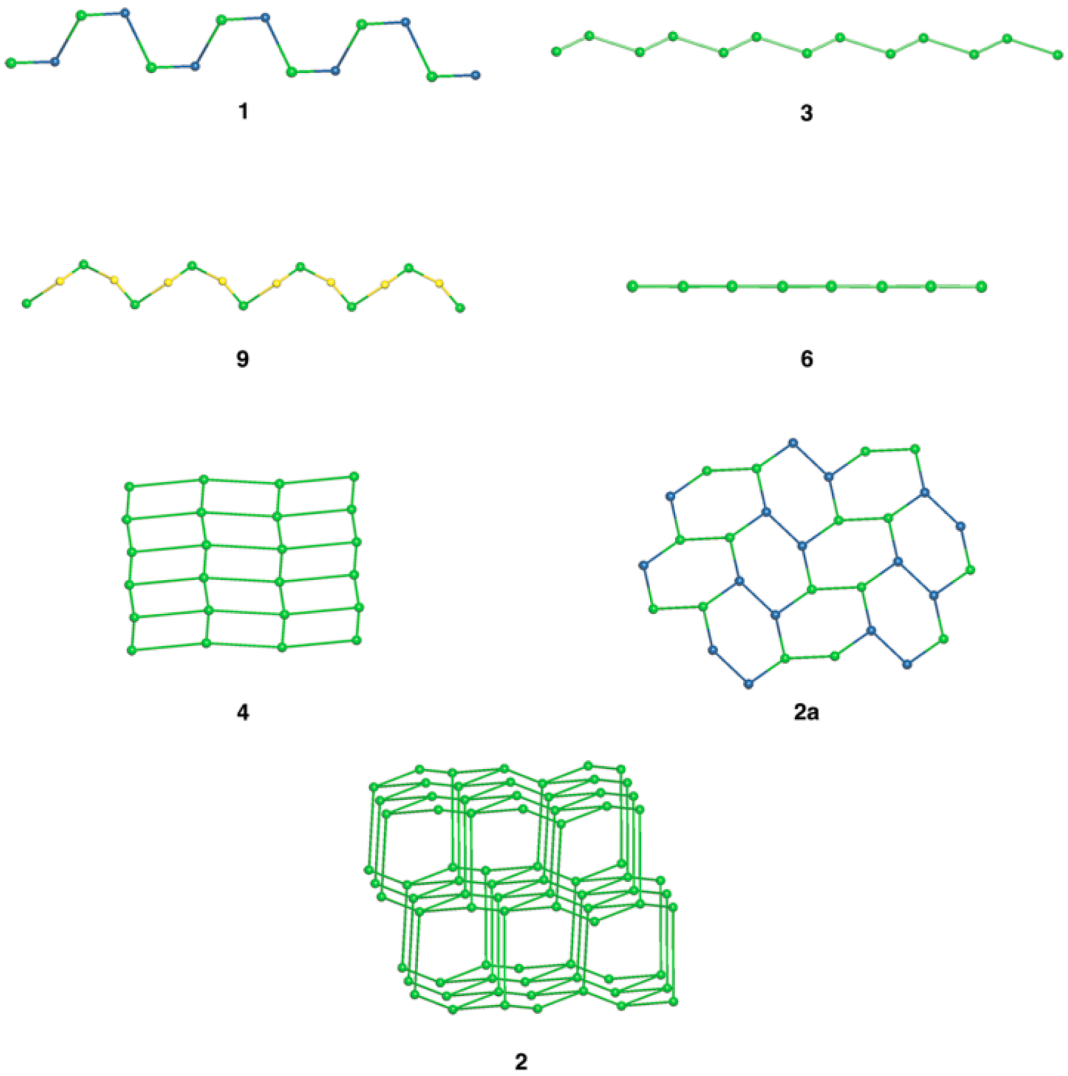

Fig. 8. Underlying nets arranged by increasing dimensionality. Green spheres in **2**, **3**, **6** and **9** represent the metal complexes; in **1** and **2a**, green spheres represent the molecules containing Zn1 and the blue ones, Zn2; and in **9**, the yellow balls represent interstitial solvent DMSO.

ν(S—O) vibration modes of the bridging sulfate group. Desulfurization of thiosemicarbazones has been observed by action of strong oxidant agents or a basic medium, both in the presence of metal ions. These processes afford sulfate ions or elemental sulfur in the reaction medium [38,61].

The ^{1}H and ^{13}C NMR spectra of H_2L^2 show the signals corresponding to its structure and confirm the formation of the new dissymmetric bis (thiosemicarbazone) ligand. The ^{1}H NMR spectra in DMSO-d_6 of complexes **1** and **5** are almost identical to that of the free ligands, suggesting their decomposition in this solvent. In the spectra of complexes **2**, **4**, **7** and **9**, the signals corresponding to the hydrazinic hydrogens have disappeared, confirming the ligand double deprotonation. In the ^{13}C NMR spectra of all the complexes, in solution or in the solid state, the signals corresponding to CN, CO and CS are shifted with respect to the free ligands, supporting their coordination as N_2OS or N_2S_2 tetradentate chelates.

3.5. Fluorescence spectroscopy

To investigate the fluorescence emission of the ligands and their complexes, fluorescence spectroscopy in the solid state was performed. The fluorescence spectra were carried out in a 250–700 nm excitation-emission range, being the maximum absorption wavelength set at 360 nm for all the compounds. The fluorescence spectra of H_2L^1 and its complexes are shown in Fig. 9. As it can be observed, the free ligand shows an emission peak around 448 nm, but after formation of the complexes, the fluorescence emission was completely quenched in complexes **1**, **3** and **4**. Usually, fluorescence quenching of a ligand by complex formation is a familiar phenomenon, which is explained by processes such as electronic energy transfer, electron transfer, magnetic perturbation, redox activity, etc [62]. and it is well established that metal ions such as Ni(II) and Cu(II) tend to quench the fluorescence emission, whereas this effect is not usually observed, or at least not so strongly, with Zn(II) or Cd(II) [63,64]. Complex **2** presents higher fluorescence intensity than the free ligand, with a maximum emission peak around 568 nm. In order to justify this, it is necessary to take into account two effects, the Photoinduced Electron-Transfer (PET) and the Chelation Enhanced Fluorescence Effect (CHEF). In the PET mechanism, caused by radiation, the lone electron pairs on neighbour donor atoms, such as nitrogen or oxygen, are transferred to the π system of the fluorophore ring decreasing the fluorescence. But if these lone pairs are involved in the bonding to a metallic ion, the PET quenching effect is reduced, giving rise to the CHEF effect, where the metal ions coordinated to the ligand produce an increase in the fluorescence intensity [62,65,66]. Therefore, the observed fluorescence of complex **2**, with the ligand doubly deprotonated, is caused by a strong CHEF effect. In addition, a red shift of the wavelength of the emission maximum from 448 nm to 568 nm can be observed for complex **2** (Fig. 9a). This red shift in the emission peak is due to the complex formation, which affects the energy transition largely.

Fig. 9b shows the fluorescence spectra of H_2L^2 and their complexes. The free ligand does not present fluorescence but the zinc complexes **5**, **6** and **7** are fluorescent with a maximum emission peak around 536 nm for all of them, what can be explained again by a strong CHEF effect.

The high increase observed in the Zn(II) complexes **2**, **5** and **6** could be related to their stronger chelation, compared to those Zn(II) complexes which showed a quenching of the fluorescence emission, leading to an enlargement of the C═S and C═O bond distances (Supplementary Information) and therefore to a decrease of the Zn-O and Zn-S bond distances (Tables 3 and 4).

3.6. Photocatalytic degradation of methyl orange (MO)

The photocatalytic activity of the copper and nickel complexes has been analyzed by evaluating the decomposition of MO in aqueous solution under UV–vis irradiation. Fig. 10 shows the photoactivity for the four complexes. As observed, the complexes effectively degrade the organic dye, evidencing the photoactivity of all the tested materials. Both nickel complexes show a similar degradation ratio, but the rate is slower than for the copper complexes. Within the copper complex, compound **3**, containing the thiosemicarbazone/hydrazone ligand, displays the faster degradation profile. On the other hand, no new bands are observed by UV–vis spectroscopy in the range from 250 nm to 800 nm, which confirms the complete mineralization of methyl orange (Fig. 10b).

4. Conclusions

A new dissymmetric bis(thiosemicarbazone) ligand H_2L^2 containing 4-isopropyl-3-thiosemicarbazone and 4-(1-naphthyl)-3-thiosemicarbazone branches has been prepared and characterized. The reactivity of this ligand and the hybrid thiosemicazone/hydrazone H_2L^1 with zinc(II), copper(II) and nickel(II) nitrates in the presence of different amounts of lithium hydroxide has been explored. Five new Zn (II) complexes with different degrees of ligand deprotonation, two from H_2L^1 (**1**, **2**) and three from H_2L^2 (**5**, **6**, **7**), have been synthesized and characterized. However, by reaction with copper(II) and nickel(II), only complexes with the ligand fully deprotonated are obtained (**3**, **4**, **8**, **9**), so the degree of deprotonation of the ligands cannot be selectively controlled. However, monomeric, dimeric and polymeric structures are found. The presence of different number of NH groups, together with the presence of nitrate ions or the presence of solvent molecules, gives rise to

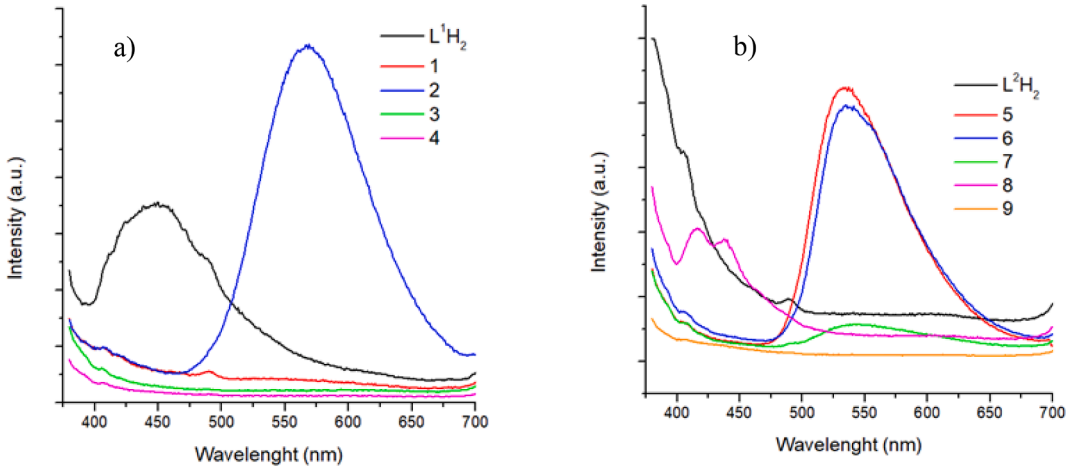

Fig. 9. Emission fluorescence spectra of a) H_2L^1 and their complexes and b) H_2L^2 and their complexes. (λ_{exc} = 360 nm).

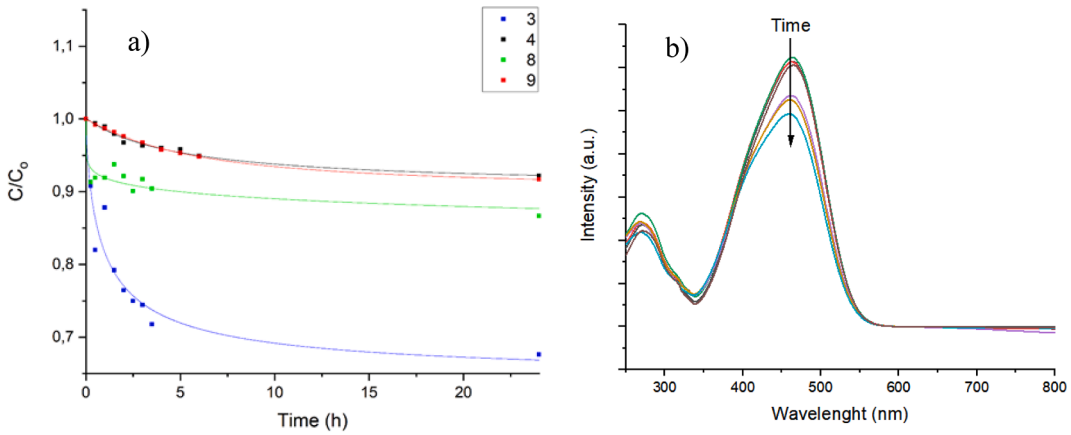

Fig. 10. a) Evolution of the methyl orange concentration with the reaction time for the copper (**3** and **8**) and nickel complexes (**4** and **9**) under UV–vis light. Results are normalized to the weight of the solids (error bars are not displayed for clarity). b) UV–Vis spectra at different times.

different hydrogen bonding arrays, which result in different supramolecular assemblies. Fluorescence emission in the solid state shows that H_2L^1 is fluorescent. This fluorescence is increased by zinc(II) complexation in complex **2**, but is completely quenched in complexes **1**, **3** and **4**. By contrast, free H_2L^2 is not fluorescent, but zinc(II) coordination causes fluorescence emission. Due to the photocatalytic activity displayed by the nickel and copper complexes, they will be tested in HER reactions in order two establish the viability of this kind of hybrid systems to act as catalysts for the clean production of hydrogen.

CRediT authorship contribution statement

Cristina González-García: Methodology. **Cristina García-Pascual:** Methodology. **Rodrigo Burón:** Methodology. **David G. Calatayud:** Investigation, Writing – review & editing. **Josefina Perles:** Investigation, Writing – review & editing. **M. Antonia Mendiola:** Conceptualization, Writing – review & editing. **Elena López-Torres:** Conceptualization, Writing – review & editing, Funding acquisition.

Declaration of Competing Interest

The authors declare that they have no known competing financial interests or personal relationships that could have appeared to influence the work reported in this paper.

Acknowledgements

The authors thank MICINN (Project PID2019-104118RB-C21) and Instituto de Salud Carlos III (Project PS09/00963) for funding.

Appendix A. Supplementary data

CCDC numbers 2154184 for HA^{i}PrTSC and 2154189-2154196 the complexes 1, 2, 2a, 3, 4, 6, 7 and 9 respectively, contains the supplementary crystallographic data for this paper. These data can be obtained free of charge via https://www.ccdc.cam.ac.uk/conts/retrieving.html, or from the Cambridge Crystallographic Data Centre, 12 Union Road, Cambridge CB2 1EZ, UK; fax: (+44) 1223-336-033; or e-mail: deposit@ccdc.cam.ac.uk. Supplementary data to this article can be found online at https://doi.org/10.1016/j.poly.2022.115945.

References

[1] H. Kaur, M. Gupta, Int. J. Pharm. Chem. Biol. Sci. 8 (2018) 259–265.
[2] D.S. Kalinowski, P. Quach, D.R. Richardson, Future Med. Chem. 1 (2009) 1143–1151.
[3] V. Rodríguez-Fanjul, E. López-Torres, M.A. Mendiola, A.M. Pizarro, Eur. J. Med. Chem. 148 (2018) 372–383.
[4] P. Khanvilkar, S.R. Dash, D. Banerjee, A. Vohra, R. Devkar, D. Chakraborty, Appl. Organomet. Chem. 35 (2021) e6343.
[5] C. Huedo, F. Zani, M. A. Mendiola, S. Pradhan, C. Sinha, E. López-Torres, *Appl. Organomet. Chem.*, 2019, **33**, e-s4700.
[6] T.S. Lobana, S. Indoria, H. Sood, D.S. Arora, M. Kaur, J.P. Jasinski, Dalton Trans. 50 (2021) 6823–6833.
[7] V. Gutsanu, G. Lisa, Polyhedron 191 (2020), 114800.
[8] A.B.M. Ibrahim, M.K. Farh, P. Mayer, Appl. Organomet. Chem. 33 (2019) e4883.
[9] A.K. Moharana, R.N. Dash, B.B. Subudhi, Mini Rev. Med. Chem. 20 (2020) 2135–2152.
[10] V. Francesconi, E. Cichero, S. Schenone, L. Naesens, M. Tonelli, Molecules 25 (2020) 1487.
[11] D. Rogolino, A. Bacchi, L. De Luca, G. Rispoli, M. Sechi, N.A. Stevaert, N. Lieve, M. Carcelli, J. Biol. Inorg. Chem. 20 (2015) 1109–1121.
[12] B. Atasever Arslan, B. Kaya, O. Sahin, S. Baday, C.C. Saylan, B. Ulkuseven, J. Mol. Struct. 1246 (2021), 131166.
[13] F. Salsi, G. Bulhoes Portapilla, K. Schutjajew, M. Roca Jungfer, A. Goulart, A. Hagenbach, S. de Albuquerque, U. Abram, Eur. J. Inorg. Chem. (2019) 4455–4462.
[14] M. Adams, Y. Li, H. Khot, C. De Kock, P.J. Smith, K. Land, K. Chibale, G.S. Smith, Dalton Trans. 42 (2013) 4677–4685.
[15] C.J. Parkinson, G.W. Birrell, M. Chavchich, D. Mackenzie, R.K. Haynes, C. de Kock, D.R. Richardson, M.D. Edstein, J. Antimicrob. Chemother. 74 (2019) 2965–2973.
[16] A. Noor, D.J. Hayne, S.C. Lim, J.K. Van Zuylekom, C. Cullinane, P.D. Roselt, C. A. McLean, J.M. White, P.S. Donnelly, Inorg. Chem. 59 (2020) 11658–11669.
[17] E.M. Andreozzi, J.B. Torres, K. Sunassee, J. Dunn, S. Walker-Samuel, I. Szanda, P. J. Blower, Metallomics 911 (2017) 1622–1633.
[18] B.M. Paterson, P.S. Donnelly, Chem. Soc. Rev. 40 (2011) 3005–3018.
[19] S. Argibay-Otero, L. Gano, C. Fernandes, A. Paulo, R. Carballo, E.M. Vázquez-López, J. Inorg. Biochem. 203 (2020), 110917.
[20] J.R. Dilworth, R. Hueting, Inorg. Chim. Acta 389 (2012) 3–15.
[21] V.S. Prado, R.C.F. Leitao, F. Silva, L. Gano, I.C. Santos, F.L.N. Marques, A. Paulo, V. M. Deflon, Dalton Trans. 50 (2021) 1631–1640.
[22] G.L. Parrilha, R.G. dos Santos, H. Beraldo, Coord. Chem. Rev. 458 (2022), 214418.
[23] M. Ranjani, P. Kalaivani, F. Dallemer, S. Selvakumar, T. Kalpana, R. Prabhakaran, Inorg. Chim. Acta 530 (2022), 120683.
[24] M. Arooj, M. Zahra, M. Islam, N. Ahmed, A. Waseem, Z. Shafiq, Spectrochim. Acta A Mol. Biomol. Spectrosc. 261 (2021), 120011.
[25] S. Sarkar, T. Mondal, S. Roy, R. Saha, A.K. Ghosh, S.S. Panja, New J. Chem. 42 (2018) 15157–15169.
[26] J.M. Bak, H. Lee, Macromolecules 50 (2017) 8529–8535.
[27] C. González-García, M.A. Mendiola, J. Perles, E. López-Torres, CrystEngComm 19 (2017) 1035–1044.
[28] D.G. Calatayud, E. López-Torres, M.A. Mendiola, Eur. J. Inorg. Chem. (2013) 80–90.
[29] A. Pino-Cuevas, A. Graña, U. Abram, R. Carballo, E.M. Vázquez-López, CrystEngComm 20 (2018) 4781–4792.
[30] C. Quiroga-Campano, H. Gómez-Machuca, S. Moris, H. Pessoa-Mahana, C. Jullian, C. Saitz, J. Mol. Struct. 1225 (2021), 129125.
[31] Z.-E. Chen, H. Zhang, Z. Iqbal, Spectrochim. Acta A Mol. Biomol. Spectrosc. 215 (2019) 34–40.
[32] P.S. Badekar, A.A. Kumbhar, New J. Chem. 42 (2018) 3917–3923.
[33] A. Barrozo, M. Orio, RSC Adv. 11 (2021) 5232–5238.
[34] M. Drosou, F. Kamatsos, C.A. Mitsopoulou, Inorg. Chem. Front. 7 (2020) 37–71.
[35] T. Straistari, R. Hardre, J. Fize, S. Shova, M. Giorgi, M. Reglier, V. Artero, M. Orio, Chem. Eur. J. 24 (2018) 8779–8786.
[36] A.Z. Haddad, B.D. Garabato, P.M. Kozlowski, R.M. Buchanan, C.A. Grapperhaus, J. Am. Chem. Soc. 13825 (2016) 7844–7847.
[37] M.-H. Shih, C.-L. Wu, Tetrahedron 61 (2005) 10917–10925.

[38] R. Gil-García, R. Fraile, B. Donnadieu, G. Madariaga, V. Januskaitis, J. Rovira, L. González, J. Borrás, F.J. Arnaiz, J. Garcia-Tojal, New J. Chem. 3711 (2013) 3568–3580.
[39] P.I.S. Maia, H.H. Nguyen, D. Ponader, A. Hagenbach, S. Bergemann, R. Gust, V. M. Deflon, U. Abram, Inorg. Chem. 51 (2012) 1604–1613.
[40] M. Christlieb, J.R. Dilworth, Chem. Eur. J. 12 (2006) 6194–6206.
[41] D.G. Calatayud, E. López-Torres, J.R. Dilworth, M.A. Mendiola, Inorg. Chim. Acta 381 (2012) 150–161.
[42] D.G. Calatayud, E. López-Torres, M.A. Mendiola, Polyhedron 54 (2013) 39–46.
[43] E. Sesmero, D.G. Calatayud, J. Perles, E. López-Torres, M.A. Mendiola, Eur. J. Inorg. Chem. (2016) 1044–1053.
[44] C. González-García, A. Mata, F. Zani, M.A. Mendiola, E. López-Torres, J. Inorg. Biochem. 163 (2016) 118–130.
[45] R.L. Tohamy, S.S. Ali, F. Li, K.M. Okasha, Y.A.G. Mahmoud, T. Elsamahy, H. Jiao, Y. Fu, J. Sun, Ecotoxicol. Environ. Saf. 231 (2022), 113160.
[46] M.R. Keshu, J. Yadav, C. Meenu, S. Chaudhary, U. Shanker, J. Environ. Chem. Eng. 9 (2021), 106763.
[47] M. Pasichnyk, J. Gaalova, P. Minarik, M. Vaclavikova, I. Melnyk, Sci. Rep. 12 (2022) 973.
[48] M. Das, M. Yadav, F. Shukla, S. Ansari, R.N. Jadeja, S. Thakore, New J. Chem. 44 (2020) 19122–19134.
[49] I. A. Obiora-Okafo, O. D. Onukwuli, N. C. Eli-Chukwu, *Water S.A.*, 2020, **46**, 300–312.
[50] G. Guan, E. Ye, M. You, Z. Li, Small 16 (2020) 1907087.
[51] Z. Youssef, L. Colombeau, N. Yesmurzayeva, F. Baros, R. Vanderesse, T. Hamieh, J. Toufaily, C. Frochot, T. Roques-Carmes, Dyes Pigm. 159 (2018) 49–71.
[52] M. Dai, H.-X. Li, J.-P. Lang, CrystEngComm 17 (2015) 4741–4753.
[53] G. M. Sheldrick, SADABS Version 2.03, Program for Empirical Absorption Corrections, Universität Göttingen: Göttingen, Germany, 1997–2001.
[54] G. M Sheldrick, SAINT+NT (Version 6.04) SAX Area-Detector Integration Program, Bruker AXS, Madison, WI, 1997-2001.
[55] G. M. Sheldrick, SHELXTL (Version 6.10) Structure Determination Package, Bruker AXS, Madison, WI, 2000.
[56] G.M. Sheldrick, Acta Crystallogr. Sect. A 46 (1990) 467.
[57] W.J. Geary, Coord. Chem. Rev. 7 (1971) 81.
[58] A.W. Addison, T.N. Rao, J. Reedijk, J. van Rijn, G.C. Verschoor, J. Chem. Soc., Dalton Trans. (1984) 1349.
[59] L. Yang, D.R. Powell, R.F. Houser, Dalton Trans. (2007) 955.
[60] V.A. Blatov, A.P. Shevchenko, D.M. Proserpio, Cryst. Growth Des. 14 (2014) 3576–4386.
[61] A. Castiñeiras, S. Dehnen, A. Fuchs, I. García-Santos, P. Sevillano, *Dalton Trans.*, 2009, 2731–2739; (b) A. Castiñeiras, I. García-Santos, *Z. Anorg. Allg. Chem.*, 2008, **634**, 2907–2916.
[62] S. Konar, A. Jana, K. Das, S. Ray, S. Chatterjee, J.A. Golen, A.L. Rheingold, S.K. Kar, Polyhedron 30 (2011) 2801–2808.
[63] C. Sun, S. Du, T. Zhang, J. Han, Front. Chem. 9 (2021), 766442.
[64] V. Gomathi, R. Selvameena, Inorg. Chim. Acta 480 (2018) 42–46.
[65] N.J. Williams, W. Gan, J.H. Reibenspies, R.D. Hancock, Inorg. Chem. 48 (2009) 1407–1415.
[66] J.R. Lakowicz, Principles of Fluorescence Spectroscopy, third ed., Springer Science + Business Media, New York, 2006.